scientific reports

Check for updates

OPEN

Potential value of novel multiparametric MRI radiomics for preoperative prediction of microsatellite instability and Ki-67 expression in endometrial cancer

Zhichao Wang[1,2], Yan Hu[1,2], Jun Cai[1], Jinyuan Xie[3], Chao Li[1], Xiandong Wu[1], Jingjing Li[1], Haifeng Luo[1]✉ & Chuchu He[1]✉

Exploring the potential of advanced artificial intelligence technology in predicting microsatellite instability (MSI) and Ki-67 expression of endometrial cancer (EC) is highly significant. This study aimed to develop a novel hybrid radiomics approach integrating multiparametric magnetic resonance imaging (MRI), deep learning, and multichannel image analysis for predicting MSI and Ki-67 status. A retrospective study included 156 EC patients who were subsequently categorized into MSI and Ki-67 groups. The hybrid radiomics model (HMRadSum) was developed by extracting quantitative imaging features and deep learning features from multiparametric MRI using emerging attention mechanism. Tumor markers were subsequently predicted utilizing an XGBoost classifier. Model performance and interpretability were evaluated using standard classification metrics, Gradient-weighted Class Activation Mapping (Grad-CAM), and SHapley Additive exPlanations (SHAP) techniques. For the MSI prediction task, the HMRadSum model achieved area-under-curve (AUC) value of 0.945 (95% CI 0.862-1.000) and accuracy of 0.889. For the Ki-67 prediction task, the AUC and accuracy of HMRadSum model was 0.888 (95% CI 0.743-1.000) and 0.810. This hybrid radiomics model effectively extracted features associated with EC gene expression, providing potential clinical implications for personalized diagnosis, treatment, and treatment strategy optimization.

Keywords Radiomics, Attention mechanism, SHAP analysis, Endometrial cancer, Machine learning

Endometrial cancer (EC) refers to the cancer that develops in the epithelial cells of the uterine endometrium in women, representing over 90% of uterine body cancers. In recent years, there has been a consistent increase in the incidence and mortality rates of EC globally[1,2]. Statistics indicate that in 2023, an estimated 66,200 new cases of uterine body cancer will be diagnosed in the United States, resulting in approximately 13,030 deaths, with the mortality rate continuing to rise annually by about 1%[1]. Early-stage EC is mainly treated with surgery, with a 3-year recurrence rate of approximately 11%, and a favorable prognosis (5-year survival rate > 95% for stage I)[3,4]. However, in cases of distant metastasis or advanced stages, personalized radiotherapy, chemotherapy, or immunotherapy may not be beneficial, leading to significant metastatic lesions (5-year survival rates of only 17% and 15% for stages IVA and IVB)[5]. The emergence of molecular diagnostics and treatments for EC has validated the potential benefits of immunotherapy for patients with high microsatellite instability (MSI) through numerous large-scale trials, making it an important biomarker to guide treatment strategies[6]. Additionally, Ki-67, as a protein indicating cellular proliferation status and biological behavior, can be used to assess the risk of recurrence and prognosis in EC[7]. MSI status may indicate the response and prognosis to tumor treatment, while the Ki-67 index also indicates the degree of tumor malignancy and thus the prognosis. Therefore, utilizing tumor biomarkers such as MSI and Ki-67 to accurately predict recurrence, metastasis, and prognosis in the early stages of cancer progression is crucial for selecting personalized treatment plans and improving the quality of life for women.

[1]Department of Oncology, The First Affiliated Hospital of Yangtze University, Jingzhou, Hubei, China. [2]Hubei Province Key Laboratory of Precision Radiation Oncology, Wuhan 430022, China. [3]Department of Joint Surgery and Sports Medicine, Jingmen Central Hospital, Jingmen, Hubei, China. ✉email: haifengrt@163.com; 584251394@qq.com

In clinical practice, MSI and Ki-67 are typically identified through immunohistochemistry (IHC) to detect mismatch repair proteins (MMR) and Ki-67 expression[6,8]. IHC is a widely used and cost-effective detection method. However, antigen expression may vary within tumors with high heterogeneity, which may lead to bias if the sampling area does not accurately reflect the tumor characteristics. Therefore, this approach is invasive, and a single sample at a specific time or location may not fully capture the heterogeneity of malignant tumors, thus limiting sampling difficulty and diagnostic effectiveness[9]. Moreover, when patients cannot undergo IHC, obtaining MSI status and Ki-67 levels becomes challenging. Therefore, the development of a non-invasive, real-time, and efficient automated approach is crucial for auxiliary assessment.

The rapid advancement of artificial intelligence technology has led to strong prospects for the integration of radiomics in decision analysis research, especially in tumor diagnosis, gene mutation detection and prognosis prediction[10]. Lefebvre utilized multiparametric MRI (including T2-weighted, Diffusion-weighted, and Dynamic contrast-enhanced MRI) to assess machine learning's performance in predicting myometrial invasion, lymph-vascular space invasion (LVSI), the international federation of gynecology and obstetrics (FIGO) stage, demonstrating superior comprehensive assessment performance compared to radiologists[11]. Lin developed a recurrence risk prediction model using MRI radiomics and clinical pathological information with XGBoost, and showed better results compared to single models[12]. Li evaluated the feasibility of predicting the survival time of EC using MRI images and clinical information, confirming the accuracy and reliability of the integrated solution[13]. Nonetheless, medical imaging features in specific application may be nonlinear, complex, and difficult to describe. Machine learning models and manual feature calculations may struggle to capture such mappings. Furthermore, current radiomics research on EC focuses on traditional histopathological feature analysis, with relatively fewer studies on predicting key immunohistochemical markers or gene mutations[14].

Deep learning has significantly enhanced the classification performance of artificial intelligence models, particularly in image analysis and adaptive feature extraction. With the growing clinical value of molecular subtyping and tumor markers, deep learning - based MRI radiomics research can effectively extract information on tumor marker expression such as MMR and Ki-67. Song developed a radiomics model for multi-sequence MRI based on three machine learning models and manual feature extraction techniques, achieving an AUC of 0.937 in predicting MSI status[15]. In predicting the four molecular subtypes of EC, Fremond developed an interpretable deep learning model for analyzing whole-slide images, with an AUC value of 0.876[16]. However, there are still limited studies on non-invasive deep learning approaches for predicting MSI or Ki-67, and the interpretability issue remains challenging, with a relatively low utilization rate of medical imaging resources.

Therefore, this study aimed to develop an innovative hybrid radiomics scheme that integrates multi-parameter MRI analysis, hybrid deep learning, and multi-channel image processing. The goal was to demonstrate the potential for predicting MMR and Ki-67 expression in EC, thereby assisting in indicating recurrence risk, treatment strategies, and prognosis.

Materials and methods

Patients

This retrospective study was approved by the Ethics Committees of the First Affiliated Hospital of Yangtze University, and the requirement for informed consent was waived. All methods were performed in accordance with the relevant guidelines and regulations. Patients were included based on the following criteria: (i) postoperative pathological diagnosis confirming EC; (ii) MRI examination conducted at our institution within 2 weeks before surgery; (iii) available medical records. Patients were excluded according to the following criteria: (i) treatment history (radiotherapy, chemotherapy or other treatments) before MRI; (ii) lack of Ki-67 or MSI status information; (iii) MRI artifacts or tumors that were too small to substantially affect the imaging observation of the tumor and its surrounding areas. Figure 1 depicts the flowchart of patient selection. The available medical records also included patient's age, histological subtype, FIGO stage, tumor size, and other relevant details.

Identification of MSI and Ki-67 status

Following the standard IHC protocol, specimens collected within one week were utilized to determine the MSI and Ki-67 status. The criteria for determining tumor markers were as follows: (1) MSI: In clinical application, it was determined by the expression of MMR proteins. If all four proteins (MLH1, MSH2, MSH6, and PMS2) were expressed, the tumor was described as microsatellite stability (MSS). When at least one MMR protein was not expressed, the tumor was defined as MSI. (2) Ki-67: IHC was performed to determine the Ki-67 score by counting the percentage of positively stained tumor cells. Positive Ki-67 expression was identified by clear brown-yellow granules within the tumor cell nuclei. Finally, the Ki-67 proliferation index was calculated based on the percentage of positive tumor cells in the hotspot area under high-power microscopy, and patients were categorized into two groups based on Ki-67 $\geq$ 50% and Ki-67 $<$ 50%.

MRI equipment parameters

Our standard MRI scans were performed using three 1.5 T scanners (Philips prodiva) and one 3.0 T scanner (Siemens Verio; Siemens Magnetom Aera) at our institution. All MRI examinations include T1 weighted imaging (T1WI) and T2 weighted imaging (T2WI). In this study, two sequences of transverse images were acquired, and the largest tumor layer along with two adjacent slices were selected as three-channel data for image analysis. Comprehensive analysis of images from multiple perspectives can be considered in further studies. The scan parameters of T2WI included repetition time (TR) and echo time (TE) of 4800 ms and 120.5 ms, a pixel matrix of 256*224, slice thickness and gap of 5 mm and 1 mm, and field of view (FOV) of 240*240 mm. T1WI was acquired with TR/TE of 550/13 ms, a pixel matrix of 256*256, thickness of 4 mm, and FOV of 360*360 mm. The scanning parameters were based on clinical diagnostic practice, so the imaging differences between different scanners were small enough not to affect model development. The scanning sequences and parameters adopted

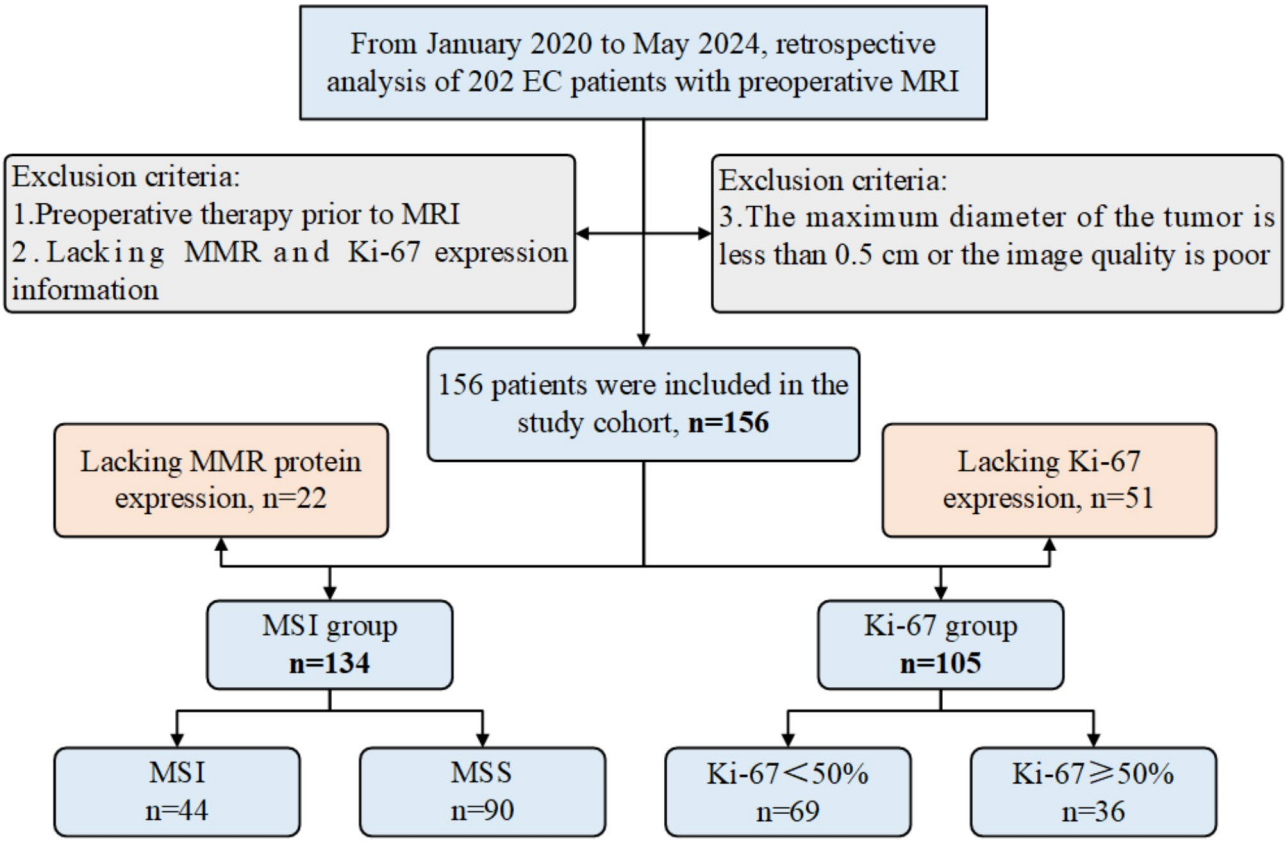

Fig. 1. Flowchart of inclusion and exclusion criteria for eligible patients.

were consistent with the clinical diagnosis of our institution to ensure the potential application significance and versatility of this work. A visual representation of these parameters is shown in Table S1.

Classical radiomics scheme

The workflow of this study is shown in Fig. 2. In the classical radiomics scheme, image acquisition and region of interest (ROI) segmentation were performed first. T1WI and T2WI images were collected and imported into ITK-SNAP3.8 software in digital imaging and communications in medicine (DICOM) format for ROI segmentation. A physician with over five years of experience in pelvic MRI imaging diagnosis manually delineated the three-dimensional ROI region layer by layer on the registered images. The segmentation contour was reviewed by a senior physician with more than 10 years of experience in radiological diagnosis, and finally a consensus on ROI segmentation was reached.

In this classical radiomics study, quantitative radiomics features were extracted from the segmented ROI region using the Pyradiomics toolbox[16]. Among the 1015 features extracted from each sequence, there were 18 first-order features, 14 shape features, 73 texture features such as gray level co-occurrence matrix (GLCM), gray level dependence matrix (GLDM), gray level run-length matrix (GLRLM), gray level size zone matrix (GLSZM) and neighborhood gray tone difference matrix (NGTDM) features, and 910 high-order features including 182 and 728 features derived from Laplacian of Gaussian (LoG) and wavelet. The Z-score and Pearson correlation coefficient were combined for data normalization and feature screening to improve the training efficiency. Pearson correlation coefficients greater than 0.9 were considered redundant, and preliminarily feature screening was then carried out. The Z-score formula is shown below.

$$Z = \frac{\mathrm{Z} - \bar{Z}}{\mathrm{s}}$$

Where, $\bar{Z}$ is the mean value of the feature Z, and s represents the standard deviation. The final feature selection was performed using the least absolute shrinkage and selection operator (LASSO), and the non-zero items in the fused features were determined as viable inputs. The preprocessed features were then used as input for training machine learning models to predict MSI or Ki-67 status.

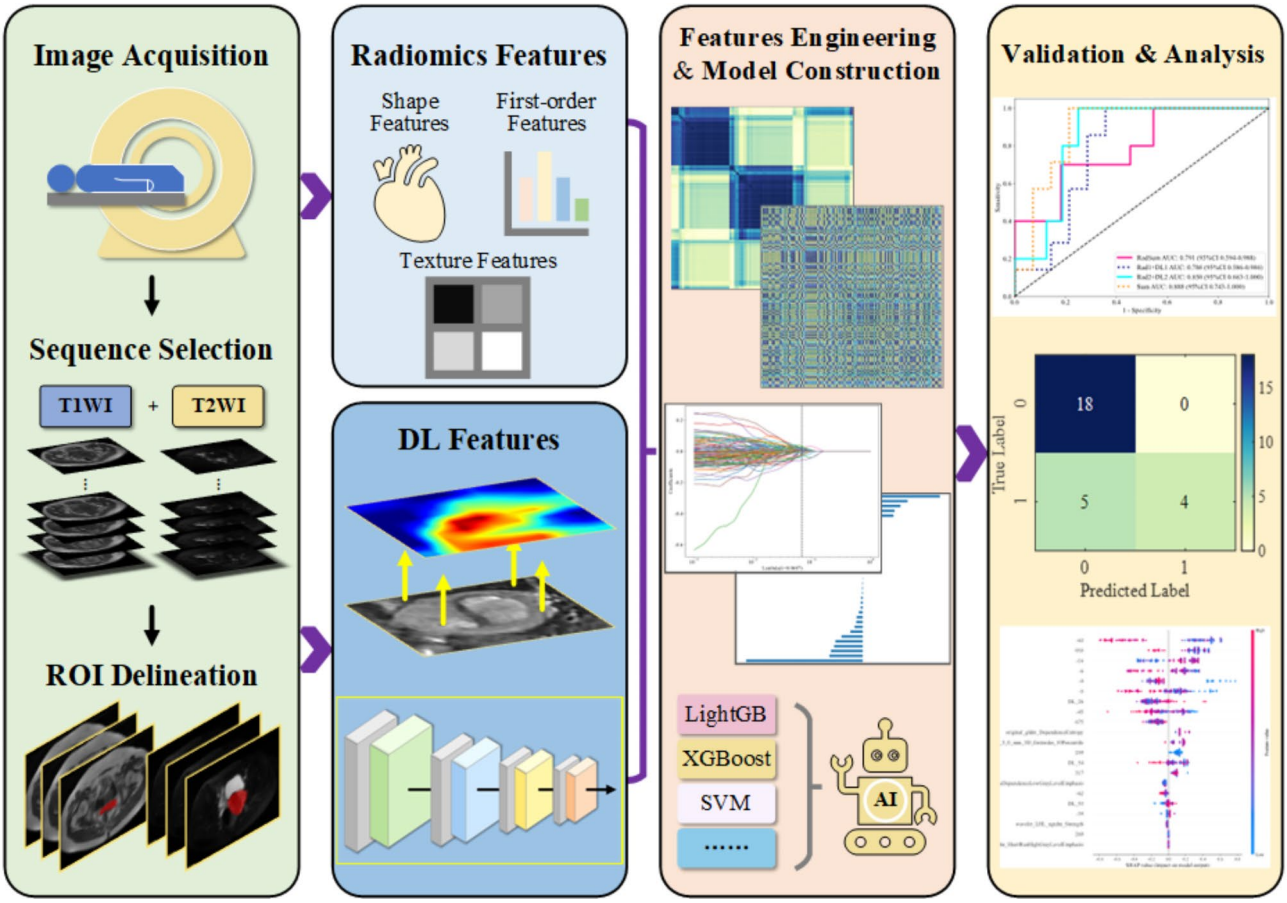

Fig. 2. Flowchart of this research study.

Hybrid radiomics scheme

As illustrated in Fig. 2, a novel hybrid radiomics scheme was proposed in this paper aimed at enhancing diagnostic performance. This scheme integrated traditional radiomics features with deep learning features, and then machine learning classifier was used to achieve high-accuracy classification.

In the data input, the selected tumor layer and its two adjacent slices were resized to 224*224 to form a 2.5D input. In recent years, due to the powerful global information representation and self-attention mechanisms, the Transformer model has achieved great breakthroughs in computer vision and image feature extraction[17]. On this basis, the CrossFormer model was employed in this paper to analyze three-channel/slices images. This model can establish an effective attention mechanism across different levels, thereby improving the cross-dimensional image processing capability, with the aim of extracting deep learning features related to MMR and Ki-67 expression[18]. The CrossFormer model (pretrained on ImageNet) integrated cross-dimensional dependencies, with high training efficiency, cross-dimensional attention mechanism, and excellent image processing performance.

In feature extraction and fusion, the parameters of the penultimate layer network nodes of the model were extracted and reduced to 64 dimensions as high-dimensional deep learning features (DLF). In the hybrid radiomics scheme, the radiomics and DLF features of T1WI and T2WI were spliced and fused. The quantitative radiomics feature extraction method was the same as classical radiomics scheme. Feature screening was performed using LASSO, and the non-zero items in the fused features were determined as viable inputs.

In classifier construction, the refined reduced-dimensional features were input into the machine learning classifier for predicting MSI and Ki-67 status. Key metrics such as AUC, accuracy (ACC), Sensitivity (SEN), and Specificity (SPE) were calculated to evaluate the classification performance of radiomics model. The machine learning models included support vector machine (SVM), light gradient boosting machine (LightGBM), and eXtreme gradient boosting (XGBoost). Binary classification results were presented using the confusion matrix. For the hybrid radiomics scheme, feature visualization and SHAP analysis were carried out to explore the interpretability of the decisions. Machine learning classification performance was compared using the AUC, ACC, SEN, and SPE metrics. Model classification performance was analyzed based on the receiver operating characteristic (ROC) curve. After the classifier for predicting tumor markers was constructed, its generalization ability was verified and analyzed based on the test set.

Statistical analysis

Statistical analysis of patient data was conducted using SPSS (version 26.0). Continuous variables were described as mean ± standard deviation, while discrete variables were reported as frequency and percentage. Continuous data were analyzed using Student's t-test and analysis of variance. Categorical data were analyzed using chi-square test and Fisher's exact test. P value < 0.05 was considered statistically significant. Data preprocessing and feature evaluation, LASSO regression analysis, and model design were performed using Python (version 3.11).

Results

Overall patient characteristics

Between January 2020 and May 2024, this study enrolled 156 patients with endometrial cancer from the First Affiliated Hospital of Yangtze University. They were divided into MSI group ($n = 134$) and Ki-67 group ($n = 105$). Within the MSI group, there were 90 cases of MSS and 44 cases of MSI. Within the Ki-67 group, there were 69 cases of Ki-67 < 50% and 36 cases with Ki-67 ≥ 50%. In the prediction of MSI and Ki-67 expression, the training set and test set were divided according to the ratio of 8:2. The baseline clinical characteristics of the patients are presented in Table 1, including histological diagnosis, demographic characteristics. No significant differences were observed in the clinical characteristics between the two groups (all $P > 0.05$), except for Differentiation in the Ki-67 group ($P = 0.023$).

Performance of radiomics scheme on different machine learning models

We compared three machine learning models, including LightGBM, SVM and XGBoost, to analyze the imaging features and predict tumor markers for endometrial cancer, and finally obtained the optimal model in this scenario. Following the classic radiomics scheme, the quantitative imaging features were manually extracted. After feature engineering and model construction, the final machine learning model results are obtained and presented in Table 2.

Table 2 presented the classification performance of models using T1WI, T2WI and their fused sequences. The selected machine learning models included LightGBM, SVM and XGBoost, named by the combination of the sequences and models. RadSum represented the XGBoost model trained by the fused sequence. In the MSI prediction based on the T1WI sequence, T1-XGBoost and T1-LightGBM achieved the same AUC. When using T2WI sequence as input, T2-XGBoost achieved a higher AUC value. More importantly, multi-sequence fused MRI provided more comprehensive imaging features, and RadSum finally achieved the highest AUC (0.753 95%CI 0.520–0.987) and ACC (0.815). In predicting Ki-67 expression based on single sequence, T1-SVM and T2-XGBoost achieved higher AUCs. Similarly, the fused sequence RadSum model achieved the highest prediction results, with an AUC of 0.791 (95%CI 0.594–0.988) and an ACC of 0.714.

The ROC curves of the models in the test set are shown in Fig. 3. To explore tumor markers prediction in detail, the confusion matrices of the RadSum model for MSI and Ki-67 predictions are shown in Fig. S1. Table S2 and Fig. S2 provide other classification performance indicators and calibration curves of the RadSum model, to more comprehensively demonstrate the effectiveness of the model. In addition, in the XGBoost model training, the setting of regularization terms and feature dimensionality reduction can effectively control the model complexity, thereby reliably preventing overfitting. Table 2; Fig. 3 demonstrate that the combination of

Parameters	MSS ($n = 90$)	MSI ($n = 44$)	*P*	Ki-67 < 50% ($n = 69$)	Ki-67 ≥ 50% ($n = 36$)	*P*
Age, years	57.60 ± 10.64	56.41 ± 9.64	0.532	58.30 ± 10.46	60.81 ± 9.97	0.141
Tumor size, cm	3.55 ± 1.99	3.88 ± 2.01	0.486	3.64 ± 2.21	3.93 ± 2.75	0.589
FIGO stage			0.628			0.620
< II	77(85.56%)	36(81.82%)		60(86.96%)	30(83.33%)	
≥II	13(14.44%)	8(18.18%)		9(13.04%)	6(16.67%)	
Differentiation			0.144			0.023
G1	42(46.67%)	12(27.27%)		25(36.23%)	7(19.44%)	
G2	40(44.44%)	27(61.36%)		38(55.07%)	19(52.78%)	
G3	8(8.89%)	5(11.36%)		6(8.70%)	10(27.78%)	
Pathological			0.481			0.089
Endometrioid	79(87.78%)	39(88.64%)		59(85.51%)	27(75.00%)	
Serous	4(4.44%)	3(6.82%)		4(5.80%)	7(19.44%)	
Others	7(7.78%)	2(4.55%)		6(8.70%)	2(5.56%)	
LVSI			0.712			0.562
Yes	13(14.44%)	5(11.36%)		7(10.14%)	2(5.56%)	
No	77(85.56%)	39(88.64%)		62(89.86%)	34(94.44%)	
Invasion depth			0.397			0.306
Deep(<1/2)	26(28.89%)	9(20.45%)		19(27.54%)	14(38.89%)	
Shallow(≥ 1/2)	64(71.11%)	35(79.55%)		50(72.46%)	22(61.11%)	

Table 1. Patient clinical characteristics.

Models	Training Cohort				Testing Cohort			
MSI	AUC	ACC	SEN	SPE	AUC	ACC	SEN	SPE
T1-Light GBM	0.896	0.766	0.939	0.689	0.670	0.667	0.455	0.812
T1-SVM	0.964	0.888	0.909	0.878	0.574	0.593	0.364	0.750
T1-XGBoost	0.950	**0.925**	**0.939**	0.919	0.670	0.593	**0.818**	0.437
T2-Light GBM	0.884	0.822	0.806	0.831	0.674	0.704	0.625	0.737
T2-SVM	0.939	0.860	0.833	0.873	0.694	0.593	0.625	0.579
T2-XGBoost	0.928	0.907	0.806	**0.958**	0.737	0.778	0.500	0.895
RadSum	**0.966**	0.897	0.914	0.889	**0.753**	**0.815**	0.444	**1.000**
Ki-67								
T1-Light GBM	0.871	0.762	0.808	0.741	0.668	0.667	0.400	0.909
T1-SVM	0.871	0.833	0.846	0.828	0.745	0.667	0.300	1.000
T1-XGBoost	0.956	0.952	0.885	**0.983**	0.709	0.667	0.300	**1.000**
T2-Light GBM	0.898	0.869	0.731	0.931	0.627	0.571	0.400	0.727
T2-SVM	0.918	0.857	0.808	0.879	0.550	0.524	0.500	0.545
T2-XGBoost	0.959	0.917	0.923	0.914	0.636	0.667	0.300	1.000
RadSum	**0.960**	**0.952**	**0.923**	0.966	**0.791**	**0.714**	**0.600**	0.818

Table 2. Results of different models in classic radiomics scheme. *The best model results are shown in bold.

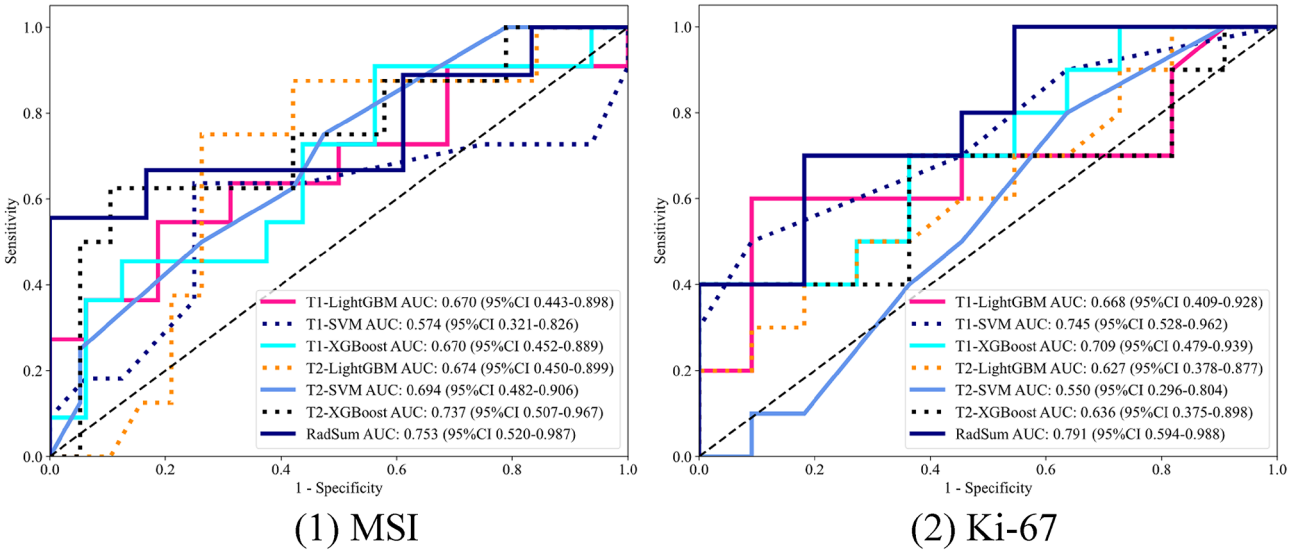

Fig. 3. ROC curves of machine learning models in classic radiomics scheme.

multi-sequence MRI and XGBoost model has the best overall performance in predicting MSI and Ki-67 of endometrial cancer.

Performance of hybrid radiomics scheme on different MRI sequences

Based on the classical radiomics scheme, the proposed hybrid radiomics scheme was investigated in this section to further improve the prediction performance. Deep learning features and radiomics features were extracted from multi-parameter MRI to comprehensively predict MSI and Ki-67 status. During deep learning model training, the largest tumor layer and its nearby layers were combined to form 2.5D dimensional input. Compared to single-channel images, multi-channel image input can comprehensively reflect the tumor features and provide the coupling relationships between the features of adjacent slices[19]. To effectively analyze three-channel images and their dependencies, the introduction of cross-dimensional attention mechanism combined with deep learning network is essential[20]. Consequently, the CrossFormer model was employed to analyze 2.5D images in this work. After obtaining the trained model, the Grad-CAM method was used to visualize the features of the network nodes, highlighting the locations that the model focused on[21]. The attention map is illustrated in Fig. 4. On the other hand, the parameters from the penultimate layer of network were extracted and reduced to

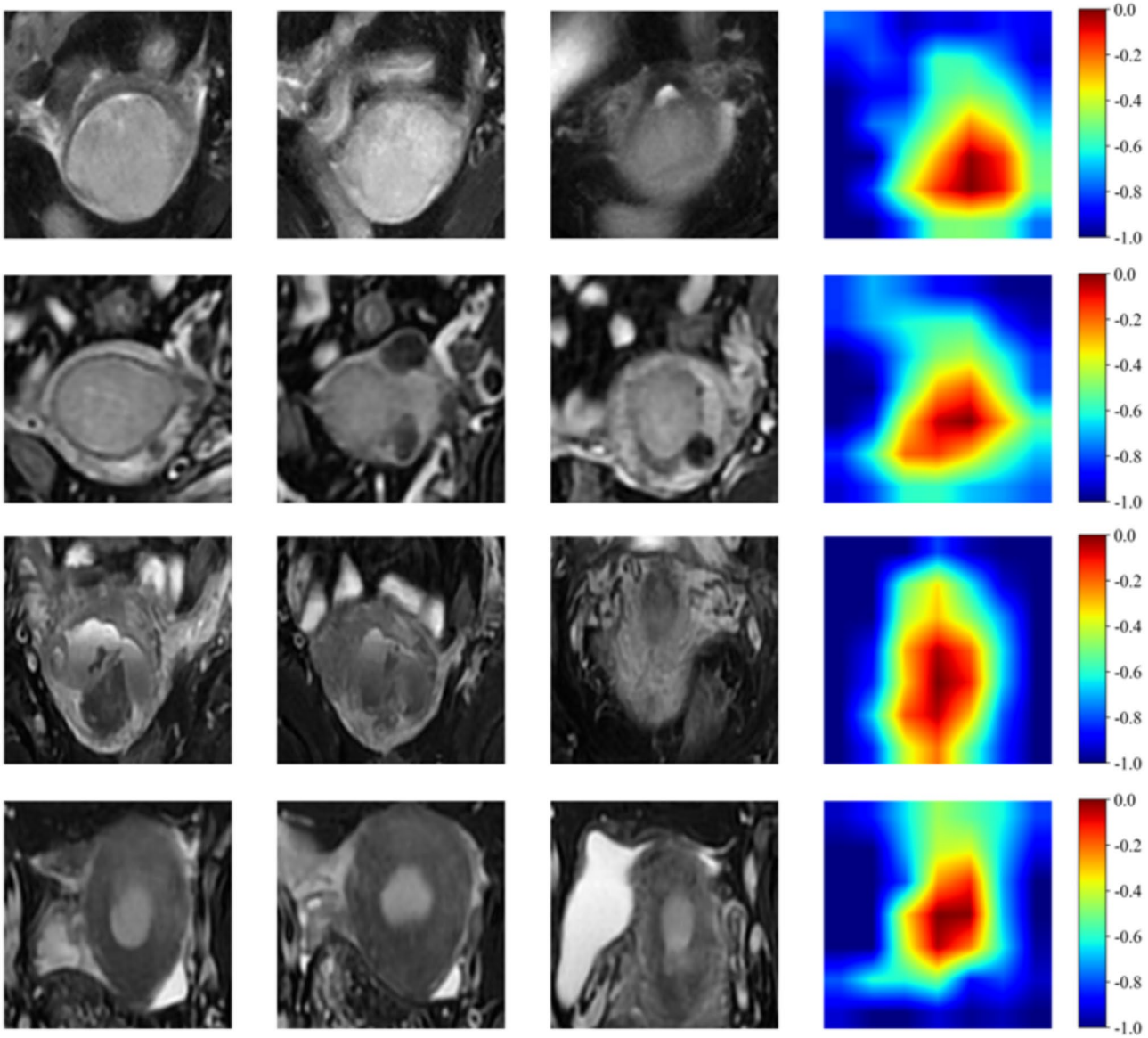

Fig. 4. Visualization of features extracted by the CrossFormer model.

64 to serve as deep learning features. After integrating the deep learning features and radiomics features, feature engineering was conducted to train the XGBoost classifier. The classification results are presented in Table 3.

The classification performance of the model with different sequence inputs were shown in Table 3. In this section, the XGBoost model was trained by the fusion of radiomics features and deep learning features. Specifically, Rad1 + DL1 and Rad2 + DL2 represented the single sequence training models of T1WI and T2WI respectively. HMRadSum represented the XGBoost model trained by the fusion of two sequences. In the MSI prediction task, the HMRadSum model achieved the best performance, attaining an AUC of 0.945 (95% CI 0.862–1.000) and an ACC of 0.889. Similarly, the HMRadSum model also demonstrated the best prediction effect in the Ki-67 prediction task, with an AUC of 0.888 (95% CI 0.743–1.000) and an ACC of 0.810. The comparison of the ROC curves in the test set is displayed in Fig. S3. In addition, Table S3 and Fig. S4 show other indicators of the hybrid radiomics scheme and the calibration curves of the HMRadSum model.

Decision explainability analysis

With significant advances of Shapley Additive exPlanations (SHAP) technology concerning interpretability, this study utilized SHAP technology to demonstrate the classification basis of the HMRadSum model[22]. Figure 5 presented the SHAP summary plot of the HMRadSum model in MSI (label = 1) status classification, offering a quantitative explanation for the decision-making process. The SHAP summary plot associated feature values with their contributions, and quantified the contribution of each feature to the classification. Features were prioritized according to their global importance. The x-axis represented the SHAP values, while the y-axis depicted the features ranked by importance, with the color indicating the feature values. Notably, the most

Models	Training Cohort				Testing Cohort			
MSI	AUC	ACC	SEN	SPE	AUC	ACC	SEN	SPE
RadSum	0.966	0.897	0.914	0.889	0.753	0.815	0.444	1.000
Rad1 + DL1	0.763	0.813	0.636	0.892	0.665	0.593	**0.818**	0.437
Rad2 + DL2	0.953	0.963	0.895	1.000	0.857	0.815	0.667	0.857
HMRadSum	**0.973**	**0.972**	**0.903**	**1.000**	**0.945**	**0.889**	0.769	**1.000**
Ki-67								
RadSum	0.960	0.952	**0.923**	0.966	0.791	0.714	0.600	**0.818**
Rad1 + DL1	0.949	0.929	0.897	0.945	0.786	0.714	0.857	0.643
Rad2 + DL2	0.833	0.762	0.742	0.774	0.850	0.762	0.800	0.750
HMRadSum	**0.983**	**0.952**	0.897	**0.982**	**0.888**	**0.810**	**0.857**	0.786

Table 3. Results of hybrid radiomics scheme on different MRI sequences. *The best model results are shown in bold.

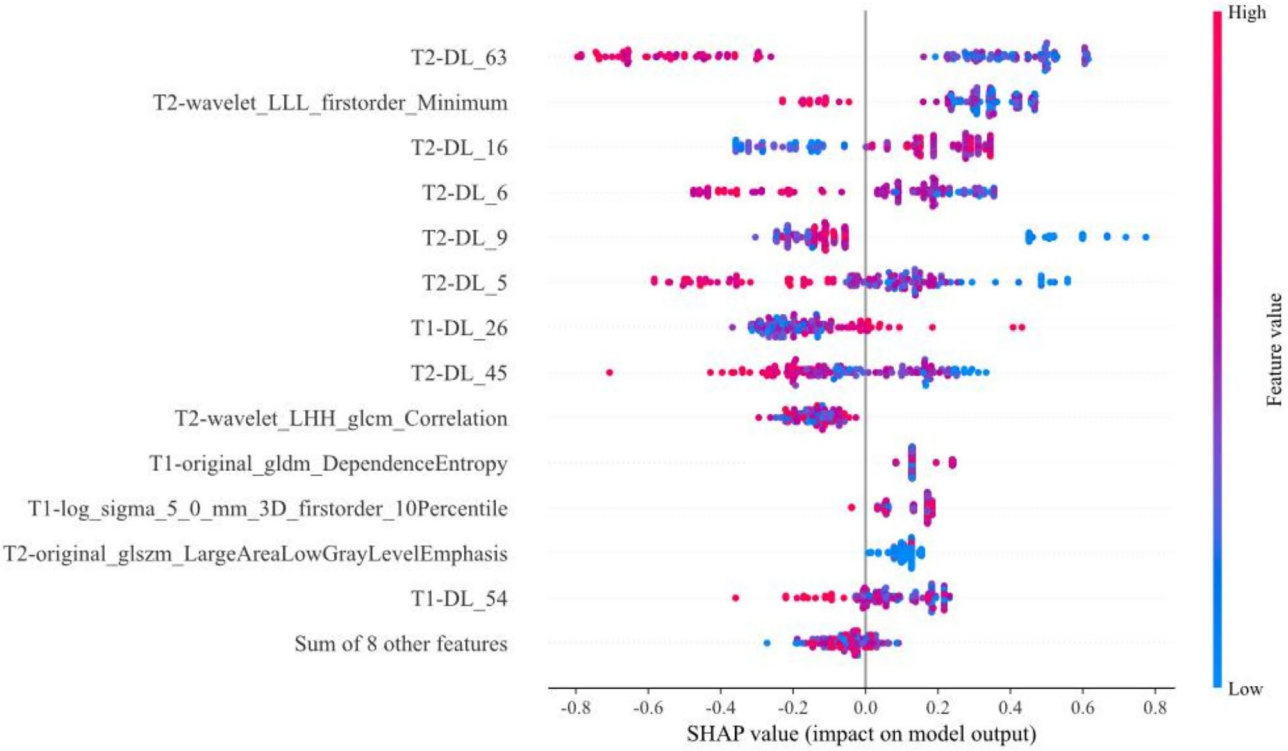

Fig. 5. SHAP summary plot of the HMRadSum model for predicting MSI.

important features in the HMRadSum model included the deep learning features of T1 and T2 sequences, the first-order features and GLCM features of T2 sequences, and the GLDM features of T1 sequences. Taking the key T2-DL_63 feature as an example, when the feature value becomes larger, the color of the sample is close to red, resulting in a smaller SHAP value, and ultimately a smaller contribution to the model output of 1, that is, a larger contribution to the output of 0. This finding provided comprehensive insights into how each feature contributed to the analysis of individual patients.

The SHAP force plots of two representative patients are shown in Fig. 6. The SHAP values started from a base value, and the final prediction value was derived by adjusting the SHAP values of each key feature. In these plots, the red arrows indicated an increased contribution of the corresponding features to predicting MSI, while the blue arrows represented a decreased contribution to MSI classification. Ultimately, through the interdependence and contributions of these key features, the final SHAP values were obtained, providing a reasoned explanation of the model's decisions for each sample.

Discussion

In this study, a hybrid radiomics scheme based on multi-sequence MRI was proposed to predict the MSI and Ki-67 status of endometrial cancer automatically. This scheme integrated multiple cutting-edge technologies,

Fig. 6. SHAP force plots explained how the HMRadSum model differentiated MMR gene expression in EC patients. The labels of patients A and B were MSI and MSS respectively. The feature value of T2-DL63 of patient A (−0.4046) was lower than that of patient B (0.0727). Combined with Fig. 5, it can be inferred that the probability of classification as MSI was increased.

including cross-dimensional attention mechanism, three-channel image processing and model interpretability analysis, to effectively extract features related to tumor marker expression. The evaluation confirmed the predictive performance of the scheme for tumor markers, with good AUC, ACC, sensitivity and specificity. Considering the reference significance and importance of MSI and Ki-67 expression for the formulation of treatment decisions in clinical practice, this work had practical significance in assisting clinical decision-making[23,24].

The application of MRI to predict the pathological characteristics and biomarkers of endometrial cancer has always been a meaningful and challenging task. This work can effectively assist clinical diagnosis and decision-making non-invasively and automatically. There is an increasing focus and interest in radiomics research to extract and analyze radiological and morphological features from MRI. Radiomics offers non-invasive, high intelligent and automated analysis, and is less affected by tumor heterogeneity. Liu combined radiomics and nomogram method to predict the lesions classification of endometrial cancer, and analyzed the most critical radiomics features[25]. Mainenti developed a radiomics model to analyze T2WI and explored the feasibility of evaluating the risk stratification of endometrial cancer using SVM[26]. Veeraraghavan developed a molecular analysis tool for endometrial cancer, utilizing machine learning to process the imaging features of enhanced CT, with AUCs of 0.78 and 0.87 on the test sets, respectively[27]. In this work, it was also found that the combination of quantitative feature calculation with machine learning can predict tumor markers to a certain extent. For instance, in the task of MSI status prediction based on RadSum model, the grey-level dependence matrix (GLDM) of the T1WI sequence and the grey-level co-occurrence matrix (GLCM) of the T2WI sequence were critical imaging features, as shown in Fig. S5. Similar to previous studies, these texture feature described information that was difficult to perceive by the naked eye, such as the specific arrangement or combination of voxels in the ROI area, and thus reflected the microscopic detail characteristics[28,29].

In this classic radiomics work, we compared the impact of different MRI sequences and models on tumor markers prediction. MRI inputs included single sequences (T1WI, T2WI) and fused sequences. Machine learning models included LightGBM, SVM and XGBoost. The radiomics workflow involved image collection and preprocessing, ROI delineation, feature extraction and screening, and machine learning construction. In the single-sequence tests, the XGBoost model achieved the best overall classification results. The AUCs of T1-XGBoost and T2-XGBoost for predicting MSI status were 0.67 (95%CI 0.452–0.889) and 0.737 (95%CI 0.507–0.967). The AUCs of T1-XGBoost and T2-XGBoost for predicting Ki-67 status were 0.709 (95%CI 0.479–0.939) and 0.636 (95%CI 0.375–0.898), respectively. More importantly, the RadSum model based on fused sequences achieved the best classification results, with AUCs of 0.753 (95%CI 0.520–0.987) and 0.791 (95%CI 0.594–0.988) for the two tasks. This revealed the significance of sufficient image information and XGBoost model for the prediction of MSI and Ki-67. Moreover, the advantages of multi-sequence MRI fusion also inspire us to find another effective approach to further enhance the prediction performance.

Recently, significant breakthroughs have been made in applying technologies such as deep learning, multi-channel image processing, and attention mechanisms to radiomics[30]. These technologies have improved efficiency

in multiple stages, including image input, feature extraction and model construction. Fremond developed a deep learning model and feature fusion strategy to analyze pathological whole-slide images, and successfully applied it to molecular subtyping and treatment outcome prediction. This work achieved breakthroughs in morpho-molecular correlations and morphological feature extraction[31,32]. Mao conducted research on image segmentation and muscle layer infiltration depth assessment based on U-Net and convolutional neural network, and verified the potential for clinical application[33]. In order to identify lymph node metastases (LNM) and LVSI in endometrial cancer, Wang constructed a deep learning scheme to analyze multi-sequence MRI, which can realize automatic tumor segmentation and pathological features prediction[34]. Similar to these studies, we observed that deep learning models demonstrated good performance in image processing and adaptive feature extraction. Feature visualization technology could alleviate the interpretability issues. Furthermore, this work integrated cross-dimensional attention mechanism, multi-channel image processing and feature fusion technology. These enhancements aimed to effectively analyze the multi-dimensional information of the tumor, and more robustly predict the MSI and Ki-67 status of endometrial cancer.

Therefore, the hybrid radiomics scheme was developed in this paper, which combined radiomics features and deep learning features to further improve the multi-task prediction performance. The deep learning model utilized the CrossFormer architecture to extract attention mechanism and image features across different tumor levels. These deep learning features were considered to be related to the expression of tumor biomarkers. Figure 4 intuitively demonstrated the attention cloud map of the CrossFormer model at the MRI level, revealing the tumor locations that the model focused on. In addition, the combination of deep learning features and radiomics features can more reliably predict the MSI and Ki-67 status. As shown in Table 3, the AUCs of Rad1 + DL1 and Rad2 + DL2 models for predicting MSI status were 0.665 (95%CI 0.455–0.874) and 0.857 (95%CI 0.679–1.000), while the results for predicting Ki-67 status were 0.786 (95%CI 0.586–0.986) and 0.850 (95%CI 0.683–1.000), respectively. More importantly, as the key model proposed in this paper, HMRadSum achieved the best classification results, with AUCs of 0.945 (95%CI 0.862–1.000) and 0.888 (95%CI 0.743–1.000) on both tasks. Compared with traditional radiomics models, the proposed HMRadSum model integrated fused features from multi-sequence MRI, and demonstrated more efficient prediction performance. This suggested that the integration of multiple cutting-edge technologies was crucial for predicting MSI and Ki-67, thereby providing valuable guidance for clinical decision support.

On another front, to address the interpretability issue of model decision, this work utilized SHAP technology to quantitatively assess the importance of features learned by the HMRadSum model. As depicted in Fig. 5, both the deep learning features and quantitative radiomics features were found to be significantly important, which verified the necessity of analyzing multi-sequence MRI and deep learning features in this work. Through two representative MSI and MSS patients, Fig. 6 intuitively showed how the key features interact with each other and finally make the correct decision from the base value. The SHAP technology illustrated the contribution of each feature to the classification, and explained the mutual coupling and influence mechanism between features, providing clinicians with insights into the potential value of this study. Therefore, this work not only achieved good results in prediction and visualization, but also provided potential application avenues for attention mechanisms in other gynecological cancers and biomarker predictions.

Of course, there are still several shortcomings in this study that need to be addressed in future research. First, multi-center (≥ 3) data verification will be added in subsequent studies to prove the generalization performance and reliability of the proposed model. Second, the sample size of the HMRadSum model is relatively small, requiring prospective for further verification. In addition, the problem of biased generalization performance due to differences in MRI equipment, geography, or technology will be studied in the future. Nonetheless, due to the visualization of quantitative radiomics features and deep learning features in this work, the hybrid radiomics scheme offers a reliable and intuitive advantage over end-to-end black box models. Finally, in the future, we will explore combining clinical parameters and images to carry out more comprehensive prediction work, and conduct comparative studies on feature extraction and visualization with other cutting-edge deep learning models.

Conclusion

In this study, we proposed a novel hybrid radiomics scheme to predict the MSI and Ki-67 status of endometrial cancer from preoperative multi-sequence MRI images. This work combined 2.5D image processing, multi-dimensional attention mechanism and deep learning to improve the prediction scheme across image input, feature fusion and model construction stages. Compared with traditional detection schemes, this work achieved breakthroughs in invasiveness, accuracy and heterogeneity, providing a highly automated and intelligent multi-task solution. Especially in scenarios where traditional IHC testing cannot be carried out, this method can effectively improve the prediction performance. SHAP technology can assisted clinicians in understanding the decision-making basis of the HMRadSum model, thereby guiding precise diagnosis and treatment. In conclusion, this study emphasized the importance of integrating multiple cutting-edge technologies to extract robust fusion features, which held significant implications for predicting endometrial cancer biomarkers and assisting in treatment plans recommendations.

Data availability

The datasets generated and/or analyzed during the current study are not publicly available due to the hospital policy regarding the use of datasets but are available from the corresponding author on reasonable request.

Received: 11 September 2024; Accepted: 23 January 2025
Published online: 25 January 2025

References

1. Siegel, R. L., Miller, K. D., Wagle, N. S. & Jemal, A. Cancer statistics, 2023. *CA Cancer J. Clin.* **73**, 17–48. https://doi.org/10.3322/caac.21763 (2023).
2. Miller, K. D. et al. Cancer treatment and survivorship statistics, 2022. *CA Cancer J. Clin.* **72**, 409–436. https://doi.org/10.3322/caac.21731 (2022).
3. Brooks, R. A. et al. Current recommendations and recent progress in endometrial cancer. *CA Cancer J. Clin.* **69**, 258–279. https://doi.org/10.3322/caac.21561 (2019).
4. Oaknin, A. et al. Endometrial cancer: ESMO Clinical Practice Guideline for diagnosis, treatment and follow-up. *Ann. Oncol.* **33**, 860–877. https://doi.org/10.1016/j.annonc.2022.05.009 (2022).
5. Makker, V. et al. Endometrial cancer. *Nat. Rev. Dis. Primers*. **7**, 88. https://doi.org/10.1038/s41572-021-00324-8 (2021).
6. Palmeri, M. et al. Real-world application of tumor mutational burden-high (TMB-high) and microsatellite instability (MSI) confirms their utility as immunotherapy biomarkers. *ESMO open.* **7**, 100336. https://doi.org/10.1016/j.esmoop.2021.100336 (2022).
7. Kitson, S. et al. Ki-67 in endometrial cancer: scoring optimization and prognostic relevance for window studies. *Mod. Pathol.* **30**, 459–468. https://doi.org/10.1038/modpathol.2016.203 (2017).
8. Stelloo, E. et al. Practical guidance for mismatch repair-deficiency testing in endometrial cancer. *Ann. Oncol.* **28**, 96–102. https://doi.org/10.1093/annonc/mdw54210.1093/annonc/mdw542 (2017).
9. Ytre-Hauge, S. et al. Preoperative tumor texture analysis on MRI predicts high-risk disease and reduced survival in endometrial cancer. *J. Magn. Reson. Imaging.* **48**, 1637–1647. https://doi.org/10.1002/jmri.26184 (2018).
10. Jiang, Y. T., Wang, C. D. & Zhou, S. T. Artificial intelligence-based risk stratification, accurate diagnosis and treatment prediction in gynecologic oncology. *Semin Cancer Biol.* **96**, 82–99. https://doi.org/10.1016/j.semcancer.2023.09.005 (2023).
11. Lefebvre, T. L. et al. Development and validation of multiparametric MRI-based radiomics models for preoperative risk stratification of endometrial cancer. *Radiology* **305**, 375–386. https://doi.org/10.1148/radiol.212873 (2022).
12. Lin, Z. J. et al. Development and validation of MRI-based radiomics model to predict recurrence risk in patients with endometrial cancer: a multicenter study. *Eur. Radiol.* **33**, 5814–5824. https://doi.org/10.1007/s00330-023-09685-y (2023).
13. Li, X. F. et al. An integrated clinical-MR radiomics model to estimate survival time in patients with endometrial cancer. *J. Magn. Reson. Imaging.* **57**, 1922–1933. https://doi.org/10.1002/jmri.28544 (2023).
14. Akazawa, M. & Hashimoto, K. Artificial intelligence in gynecologic cancers: current status and future challenges-A systematic review. *Artif. Intell. Med.* **120**, 102164. https://doi.org/10.1016/j.artmed.2021.102164 (2021).
15. Song, X. L. et al. Multisequence magnetic resonance imaging-based radiomics models for the prediction of microsatellite instability in endometrial cancer. *Radiol. Med.* **128**, 242–251. https://doi.org/10.1007/s11547-023-01590-0 (2023).
16. van Griethuysen, J. J. M. et al. Computational radiomics system to decode the radiographic phenotype. *Cancer res.* **77**, E104–E107. https://doi.org/10.1158/0008-5472.CAN-17-0339 (2017).
17. Cheng, J. H., Liu, J., Kuang, H. L. & Wang, J. X. A fully automated multimodal MRI-based multi-task learning for glioma segmentation and IDH genotyping. *IEEE T Med. Imaging.* **41**, 1520–1532. https://doi.org/10.1109/TMI.2022 (2022).
18. Wang, W. X. et al. CrossFormer plus plus: a versatile vision transformer hinging on cross-scale attention. *IEEE T Pattern Anal.* **46**, 3123–3136. https://doi.org/10.1109/TPAMI.2023.3341806 (2024).
19. Saint-Esteven, A. L. et al. A 2.5D convolutional neural network for HPV prediction in advanced oropharyngeal cancer. *Comput. Biol. Med.* **142**, 105215. https://doi.org/10.1016/j.compbiomed.2022.105215 (2022).
20. He, H. S. et al. A novel bone marrow cell recognition method based on multi-scale information and reject option. *Eng. Appl. Artif. Intel.* **133**, 108540. https://doi.org/10.1016/j.engappai.2024.108540 (2024).
21. Selvaraju, R. R. et al. Grad-CAM: visual explanations from deep networks via gradient-based localization. *Int. J. Comput. Vis.* **128**, 336–359. https://doi.org/10.1109/ICCV.2017.74 (2016).
22. Lundberg, S. M. & Lee, S. I. A unified approach to interpreting model predictions. *Adv. Neural. Inf. Process. Syst.* **30**. (2017).
23. O'Malley, D. M. et al. Pembrolizumab in patients with microsatellite instability-high advanced endometrial cancer: results from the KEYNOTE-158 study. *J. Clin. Oncol.* **40**, 752–761. https://doi.org/10.1200/JCO.21.01874 (2022).
24. Meng, Y. et al. Prognostic value of Ki-67 index in patients with endometrial stromal sarcoma. *Front. Med-Lausanne.* **8**, 823505. https://doi.org/10.3389/fmed.2021.823505 (2022).
25. Liu, J. Q. et al. Development of MRI-based radiomics predictive model for classifying endometrial lesions. *Sci. Rep-UK.* **13**, 1590. https://doi.org/10.1038/s41598-023-28819-2 (2023).
26. Mainenti, P. P. et al. MRI radiomics: a machine learning approach for the risk stratification of endometrial cancer patients. *Eur. J. Radiol.* **149**, 110226. https://doi.org/10.1016/j.ejrad.2022.110226 (2022).
27. Veeraraghavan, H. et al. Machine learning-based prediction of microsatellite instability and high tumor mutation burden from contrast-enhanced computed tomography in endometrial cancers. *Sci. Rep-UK.* **10**, 17769. https://doi.org/10.1038/s41598-020-72475-9 (2020).
28. Zhu, X. L. et al. Detection of deep myometrial invasion in endometrial cancer MR imaging based on multi-feature fusion and probabilistic support vector machine ensemble. *Comput. Biol. Med.* **134**, 104487. https://doi.org/10.1016/j.compbiomed.2021.104487 (2021).
29. Jia, Y. J. et al. Radiomics analysis of multiparametric MRI for preoperative prediction of microsatellite instability status in endometrial cancer: a dual-center study. *Front. Oncol.* **14**, 1333020. https://doi.org/10.3389/fonc.2024.1333020 (2024).
30. Prelaj, A. et al. Artificial intelligence for predictive biomarker discovery in immuno-oncology: a systematic review. *Ann. Oncol.* **35**, 29–65. https://doi.org/10.1016/j.annonc.2023.10.125 (2024).
31. Fremond, S. et al. Interpretable deep learning model to predict the molecular classification of endometrial cancer from haematoxylin and eosin-stained whole-slide images: a combined analysis of the PORTEC randomised trials and clinical cohorts. *Lancet Digit. Health*. **5** (22), e71–e82. https://doi.org/10.1016/S2589-7500 (2023).
32. Volinsky-Fremond, S. et al. Prediction of recurrence risk in endometrial cancer with multimodal deep learning. *Nat. Med.* https://doi.org/10.1038/s41591-024-02993-w (2024).
33. Mao, W., Chen, C. X., Gao, H. C., Xiong, L. & Lin, Y. P. Quantitative evaluation of myometrial infiltration depth ratio for early endometrial cancer based on deep learning. *Biomed. Signal. Proces.* **84**, 104685. https://doi.org/10.1016/j.bspc.2023.104685 (2023).
34. Wang, Y. D. et al. Fully automated identification of lymph node metastases and lymphovascular invasion in endometrial cancer from multi-parametric MRI by deep learning. *J. Magn. Reson. Imaging.* https://doi.org/10.1002/jmri.29344 (2024).

Acknowledgements

This work was supported by the Open Research Fund of Hubei Key Laboratory of Precision Radiation Oncology (jzfs016, jzfs020), Jingzhou Science and Technology Plan Project (2024LHY23, 2024HD109, 2024HD66), and the Natural Science Foundation of Hubei Province (2023AFC037).

Author contributions

Conceptualization, Z.W. and C.H.; Methodology, Z.W. and H.L.; Software, Z.W., C.L., X.W., and J.L.; Validation:

C.H., J.X., and J.C.; Formal Analysis: Y.H., H.L., and C.H.; Investigation: Z.W., J.L., and C.H.; Resources: C.H., X.W. and Y.H.; Data Curation, Y.H. and C.H.; Writing—Original Draft Preparation, Z.W. and C.H.; Visualization: Z.W. and H.L.; Supervision: Y.H. and C.H.; Project Administration, Y.H. and J.C.; Funding Acquisition, Z.W. and Y.H.

Declarations

Ethics approval and consent to participate

The retrospective study was approved by the Ethics Committees of the First Affiliated Hospital of Yangtze University (KY2023100).

Competing interests

The authors declare no competing interests.

Additional information

Supplementary Information The online version contains supplementary material available at https://doi.org/10.1038/s41598-025-87966-w.

Correspondence and requests for materials should be addressed to H.L. or C.H.

Reprints and permissions information is available at www.nature.com/reprints.

Publisher's note Springer Nature remains neutral with regard to jurisdictional claims in published maps and institutional affiliations.